(Received 3 March 2024, Accepted 12 April 2024, Scheduled 22 April 2024)

Reconfigurable Designs of Sectoral Microstrip Antennas for Wideband and Circularly Polarized Response

Venkata A. P. Chavali[1], Amit A. Deshmukh[1,*], Aarti G. Ambekar[1], Hari Vasudevan[2], and Tushar V. Sawant[1]

[1]*EXTC, SVKM's D J Sanghvi CoE, Mumbai, India*
[2]*SVKM's D J Sanghvi CoE, Mumbai, India*

ABSTRACT: Gap-coupled designs of Sectoral microstrip antenna for 90° and 45° sectoral angle are proposed for wideband and circularly polarized response. On total substrate thickness of $\sim 0.1\lambda_g$, proximity fed design of 90° Sectoral patch yields simulated bandwidth of 827 MHz (50.41%) with a peak gain of 8.1 dBi, whereas its gap-coupled configuration with parasitic 45° Sectoral patches yields simulated bandwidth of 1336 MHz (69.11%) with a peak gain of 8.0 dBi. A gap-coupled design of two 90° Sectoral patches is presented in which orthogonal directions of the fundamental mode currents over the aperture are maintained. This yields circularly polarized response with axial ratio bandwidth of 709 MHz (34.88%) which lies inside the impedance bandwidth of 1103 MHz (60.09%). It offers a peak gain of larger than 7 dBi across the axial ratio bandwidth. To achieve all these operational features using a single patch, a reconfigurable design of Sectoral patches is proposed that yields similar wideband and circularly polarized characteristics. Thus present study provides a wideband and circularly polarized design that offers either impedance bandwidth of more than 65% or axial ratio bandwidth of nearly 35%. For achieved antenna response, the proposed designs fulfill the requirements of LTE (band 65, 66, and 70) and various aeronautical service mobile satellite bands (1610–2300 MHz). Experimental validation for the obtained results is carried out that shows close matching.

1. INTRODUCTION

With numerous advantages, microstrip antenna (MSA) finds many applications in wireless communication system [1, 2]. In most of the designs, MSAs are operated in their fundamental resonant mode and thus offer broadside radiation characteristics. The bandwidth (BW) enhancement in MSA is achieved when additional resonant modes are introduced, and it is obtained by using either multi-resonator configuration employing parasitic patches or modified shapes of the radiating patch, or the resonant slots cut in the patch, or the ground plane embedded with slots employing modified shapes [3–15, 42]. In free space communication, because of multi-path propagation effects, signal undergoes changes in its polarization. To avoid the signal loss arising from the mismatch in between the polarization of incident wave and the receiver antenna polarization, circularly polarized (CP) antenna is used. The CP response in MSA is achieved either by cutting narrow slot in the patch, or by using modified patch shapes, or by embedding resonant slot inside the patch, or by using defected ground plane structures [16–25]. While catering to the multiple wireless applications using a single design, wideband CP MSA is required, and it is obtained by using a thicker substrate followed by the gap-coupled/stacked configurations, or the array designs [26–29]. By using the reconfigurable design approach employing the active devices integrated on the radiating patch, pattern reconfigurable response, compact high gain antenna design, and linearly to circularly polarized response are achieved in MSAs [30–34]. The reconfigurable design helps in achieving multiple responses while using the single patch.

In this paper, gap-coupled configurations of Sectoral MSA (S-MSA) for 90° and 45° sectoral angles are proposed for wideband and CP response. The designs are proposed in 1600–2400 MHz frequency band so as to cover LTE and various aeronautical service mobile satellite applications. The MSAs are proposed on a suspended FR4 substrate ($\varepsilon_r = 4.3$, $h = 0.16$ cm) of total thickness $\sim 0.1\lambda_g$ and fed using a proximity strip. A single patch design of 90° S-MSA offers simulated BW of 827 MHz (50.41%), whereas its gap-coupled design with two 45° S-MSAs yields simulated BW of 1336 MHz (69.11%). Both the configurations yield broadside radiation characteristics with a peak gain around 8 dBi. Further, a gap-coupled design of two 90° S-MSAs of unequal radii is presented. With an orthogonal surface current variations across the two Sectoral patches at the fundamental mode, this gap-coupled antenna offers CP characteristics. It offers axial ratio (AR) BW of 709 MHz (34.88%) that lies inside the impedance BW of 1103 MHz (60.09%). Across the AR BW, gap-coupled 90° S-MSAs offers a peak gain of greater than 7 dBi. To achieve wideband and CP characteristics using a single patch, a reconfigurable configuration of four unequal radii 45° Sectoral patches is presented. The radius in each 45° Sectoral patch is selected such that based on the activation of RF diodes, respective gap-coupled design realized using composite 90° or individual 45° angle Sectoral patches, yields respective wideband linear polarized or CP response. The activation of radio frequency (RF)

* Corresponding author: Amit A. Deshmukh (amitdeshmukh76@gmail.com).

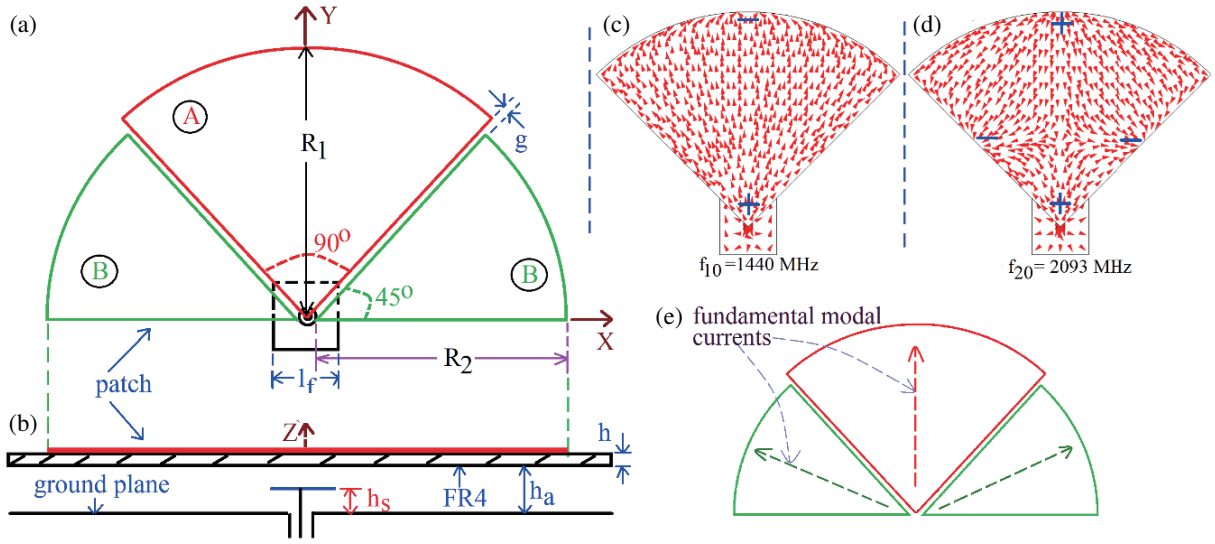

FIGURE 1. Gap-coupled design of 90° S-MSA with 45° S-MSAs (a) top and (b) side views, (c), (d) surface current distributions at first two resonant modes for 90° S-MSA, (e) fundamental mode current directions on fed and parasitic S-MSAs.

diodes helps in switching in between the wideband to CP characteristics. To highlight the technical novelty in proposed work, a comparison is presented against the reported wideband, CP, and reconfigurable configurations. It brings out that for a single patch configuration, the proposed designs offer better results in terms of realized impedance and AR BW, peak gain for the given antenna volume. The MSAs discussed in this paper are first optimized using IE3D simulations [41]. An experimental verification for the simulated results is carried out inside the antenna laboratory using ZVH-8, FSC 6 and SMB 100 A. Square ground plane of side length 30 cm using N-type connector feed of inner wire diameter 0.32 cm is selected. A close agreement is obtained between the simulation and measurements.

2. WIDEBAND DESIGNS OF PROXIMITY FED 90° AND 45° S-MSAS

Wideband design of gap-coupled 90° S-MSA with parasitic 45° S-MSAs is shown in Figs. 1(a) and (b). The patches are fabricated on the top side of an FR4 substrate, and it is suspended above the ground plane using an air gap of h_a cm. In wideband antennas, direction of the E-plane should be unchanged across the impedance BW, and the cross polar components should be at least 8–10 dB lower in magnitude than the co-polar level of radiation [1, 2]. This provides linear or elliptical polarization condition across the BW as needed in the wideband design. Initially, proximity fed 90° S-MSA is optimized for the BW. On total substrate thickness of 2.06 cm ($h_a = 1.9$ cm, $\sim 0.1\lambda_g$), 90° S-MSA radius is selected such that it resonates in the fundamental mode frequency around 1500 MHz. For these parameters, patch radius is found to be $R_1 = 8$ cm. For the proximity feed below the patch vertex as mentioned in Fig. 1(a), surface currents at the fundamental mode show one-half wavelength variation along the patch radius, as mentioned in Fig. 1(c). With this variation, fundamental mode in 90° S-MSA is referred to as TM_{10} [35, 36]. For the same feed position, next resonant mode in 90° S-MSA is TM_{20} at which surface currents exhibit two-half wavelength variations along the patch radius as mentioned in Fig. 1(d) [35, 36]. Thus across the first two resonant modes, surface currents are vertically (radial) directed leading to the direction of E-plane along $\phi = 90$. With optimization in the proximity strip length, its position below the patch and thickness for the same, maximum possible impedance BW in 90° S-MSA is achieved, and its results are shown in Fig. 2(a). The BW observed in the simulation is 827 MHz (50.41%) whereas that obtained in the measurement is 847 MHz (51.76%). The antenna offers broadside radiation characteristics with a peak gain above 8 dBi.

To increase the BW multi-resonator concept is used as it is simple in implementation. The parasitic Sectoral patches of equal radius and angle 45° are gap-coupled to the fed 90° S-MSA as shown in Fig. 1(a). On the fed and parasitic patches, radial fundamental mode is present as shown in Fig. 1(e). Hence with the addition of parasitic patches, effective direction of the radiated electrical field vector is along the $\phi = 90°$, thus maintaining the direction of E-plane along the same direction. This satisfies the requirement of wideband antennas. The wideband response is governed by the difference in the radius of fed and parasitic sectoral patches and an air gap between them. To optimize the BW, a parametric study for the variations in these parameters is carried out, and resonance curve plots and Smith charts for the same are shown in Figs. 2(b) and (c). An increase in parasitic sectoral patch radius 'R_2' tunes its TM_{10} mode frequency with reference to fed patch TM_{10} mode frequency, and air gap 'g' between them alters the loop size formed due to the gap-coupling between the respective resonant modes. An optimum response for maximum possible impedance BW is obtained for the antenna parameters as $R_1 = 8.0$, $R_2 = 6.0$, $l_f = 1.7$, $h_s = 1.5$, $h_a = 1.9$ cm. The gap-coupled antenna offers simulated and measured impedance BWs for $S_{11} \leq -10$ dB of 1336 MHz (69.11%) and 1366 MHz (70.77%), respectively as shown in Fig. 2(a). Over the S_{11} BW, antenna offers the gain

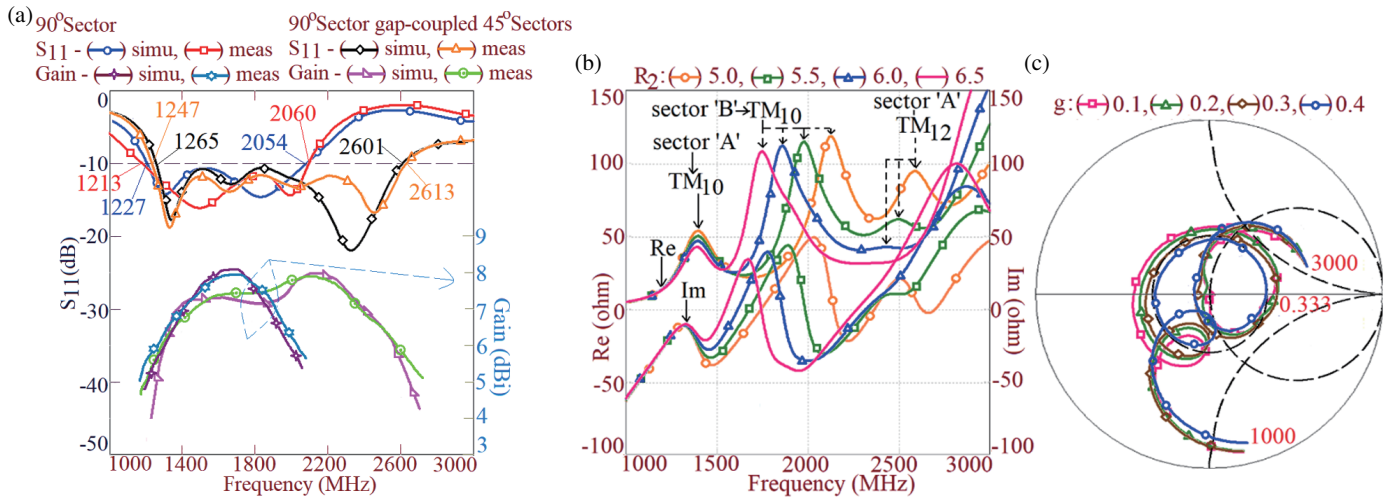

FIGURE 2. (a) Reflection coefficient (S_{11}) BW and gain plots for 90° S-MSA and gap-coupled 90° S-MSA with 45° S-MSAs, (b) resonance curve and (c) smith chart for gap-coupled 90° S-MSA with 45° S-MSAs.

of above 6 dBi with maximum value of 8 dBi. The radiation pattern across the complete BW as shown in Fig. 3 is in the broadside direction with E-plane aligned along $\phi = 90°$. An increase in the cross polar component of the radiation towards the higher frequencies of the BW is attributed to the increment in orthogonal surface current components on parasitic 45° S-MSAs.

3. GAP-COUPLED DESIGN OF 90° S-MSAS FOR WIDEBAND CP RESPONSE

The fundamental TM_{10} mode is radial in the direction on 90° S-MSA. A CP response can be realized if an additional resonator is placed nearer the fed 90° S-MSA that has orthogonal radial mode with reference to the fed patch. This arrangement is realized in the gap-coupled design of two 90° S-MSAs as shown in Fig. 4(a). The TM_{10} modes on the two patches are orthogonal to each other, which will realize the CP response. To achieve the maximum possible AR BW, an optimum frequency spacing between the two TM_{10} modes is needed. This is obtained by employing the parametric study for the variation in the radius of gap-coupled 90° S-MSAs, dimensions of the proximity strip, and its position below the patch, and maximum AR BW in the gap-coupled design is achieved. The antenna parameters in the optimum CP design are $R_1 = 8.0$, $R_2 = 6.0$, $g = 0.4$, $l_f = 1.7$, $x_f = 0.1$ cm, and the results are given in Fig. 4(b). The antenna offers simulated and measured $S_{11} \leq -10$ dB BWs of 1103 MHz (60.09%) and 1128 MHz (61.57%), respectively. The simulated and measured CP BWs for AR ≤ 3 dB, which lies inside the impedance BW, are 709 MHz (34.88%) and 751 MHz (37.12%), respectively. The antenna gain across the AR BW is above 6 dBi with maximum value above 7 dBi. With the radial orthogonal modes on the two 90° S-MSAs, the AR BW and gain are achieved in the direction $\phi = 0°$, $\theta = 30°$, i.e., away from the broadside direction. This direction will just require reorientation of the antenna along θ axis, when it works as the receiver. The simulated surface current distributions across the AR BW on the gap-coupled 90° S-MSAs were studied. They appeared orthogonal to each other across the complete AR BW. The time varying surface current distribution at the center frequency of AR BW, radiation pattern plots near the band start and stop frequencies of AR BW, input impedance, gain, and radiation pattern measurement setup are provided in Figs. 4(c), 5, and 6.

The pattern exhibits a broadside radiation with a higher cross polar level when the difference between co and cross polar levels is less than 10 dB. In CP designs, due to the presence of orthogonal resonant modes, surface currents over the aperture are bi-directional. With this, radiation pattern shows equal contribution from the co and cross polar components of radiation. With reference to the antenna as a radiator, surface currents over the patch against time rotate in the anticlockwise direction thus realizing the left hand CP (LHCP) wave. Due to this left hand field components are larger in magnitude in the simulated polarization plots. The radiation pattern plots, surface current distribution across the frequencies and over a time at a given frequency, confirm the presence of CP wave in the proposed gap-coupled antenna. The antenna impedance response is measured using vector network analyzer (VNA) ZVH-8. The radiation pattern and gain measurement are carried out inside the antenna lab wherein reference wideband horn antenna was selected in the measurement. The spectrum analyzer FSC 6 and RF source SMB 100A is used here. A far-field distance as calculated with reference to the higher frequency of AR BW is kept between the antenna under test (AUT) and reference horn antenna. The antenna gain is measured using three-antenna method to achieve a better accuracy for the measurements inside the antenna laboratory.

4. RECONFIGURABLE GAP-COUPLED SECTORAL MSA EMPLOYING FOUR 45° SECTORS

The gap-coupled S-MSAs presented in previous sections for respective wideband and CP response are optimized individually. Instead of designing multiple antennas for the wideband or CP response, a reconfigurable design of S-MSA that can of-

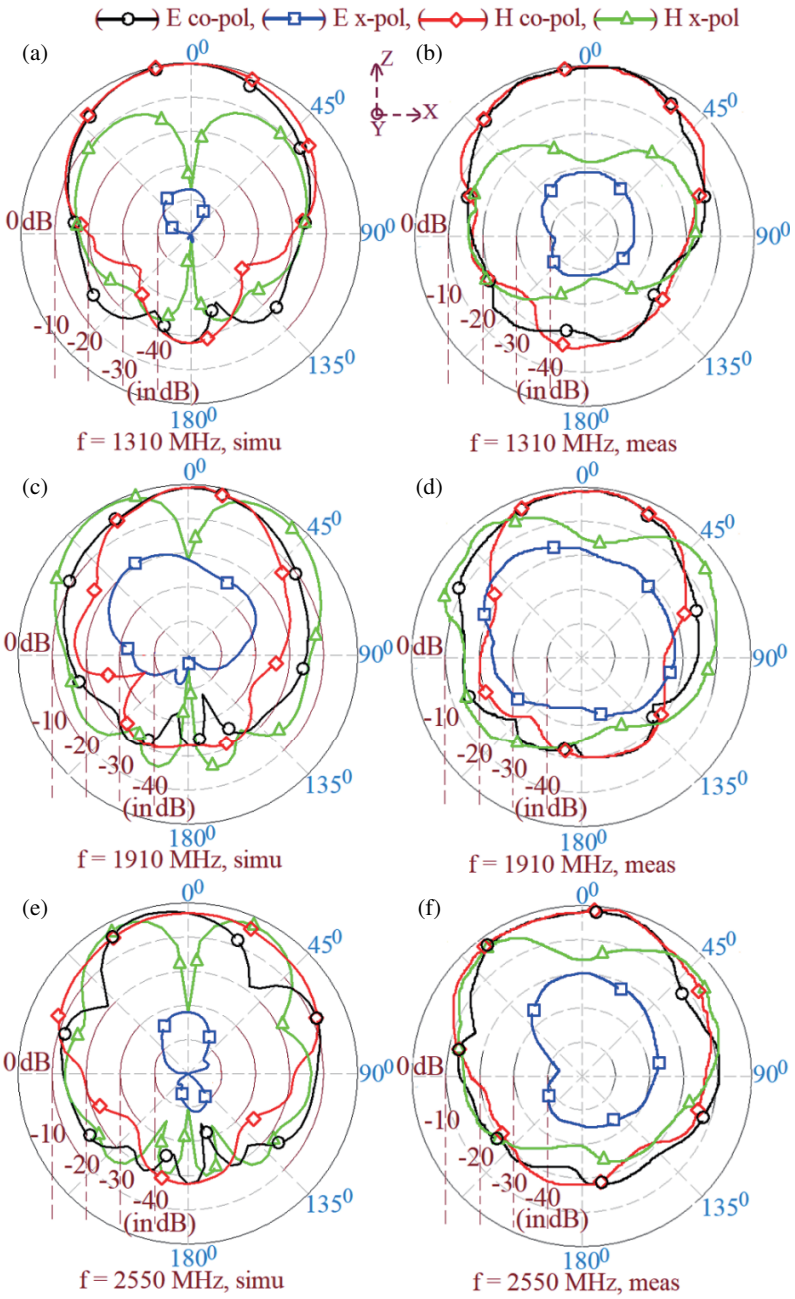

FIGURE 3. (a)–(f) Radiation pattern over the S_{11} BW for gap-coupled design of 90° S-MSA with 45° S-MSAs.

fer wideband or CP response, through the appropriate selection of the active devices, is proposed here. The reconfigurable properties are achieved by employing the RF PIN diodes. The various configurations proposed above consist of 90°, 45° Sectoral patches. Therefore, reconfigurable design is initiated by using four 45° Sectoral patches as shown in Fig. 7(a). The RF PIN diodes (BAR64-06W H6327) are connected in between the adjacent 45° sectors of the gap-coupled configuration. The DC biasing for the RF PIN diodes to realize different Sectoral patches for various configurations is achieved through the RFC (ELT3KN131B) that also ensures the isolation between the RF signal and DC biasing signal. With the suitable excitation of the RF PIN diodes, the individual gap-coupled antennas consisting of 90° and 45° patches are realized. However, the connection between the adjacent 45° Sectors is present at three points where the RF diodes are present. These individual connections against the complete connection between the 45° patches alters the current path and changes the impedance variation over the individual Sectoral patches. Due to this radius of each 45° Sectoral patch is parametrically changed such that respective wideband or CP response is achieved in each design for the given RF PIN diode excitations. The final dimensions of the 45° Sectoral patches and proximity feed in the reconfigurable antenna are $R_1 = 8.0$, $R_2 = 6.0$, $R_3 = 7.0$, $R_4 = 6.0$, $x_f = 0.7$, $l_f = 1.4$, $h_a = 1.9$, $h_s = 1.5$, $g_1 = 0.3$, $g_2 = 0.4$, $g_3 = 0.3$ cm. To realize the wideband design of 90° S-MSA gap-coupled with

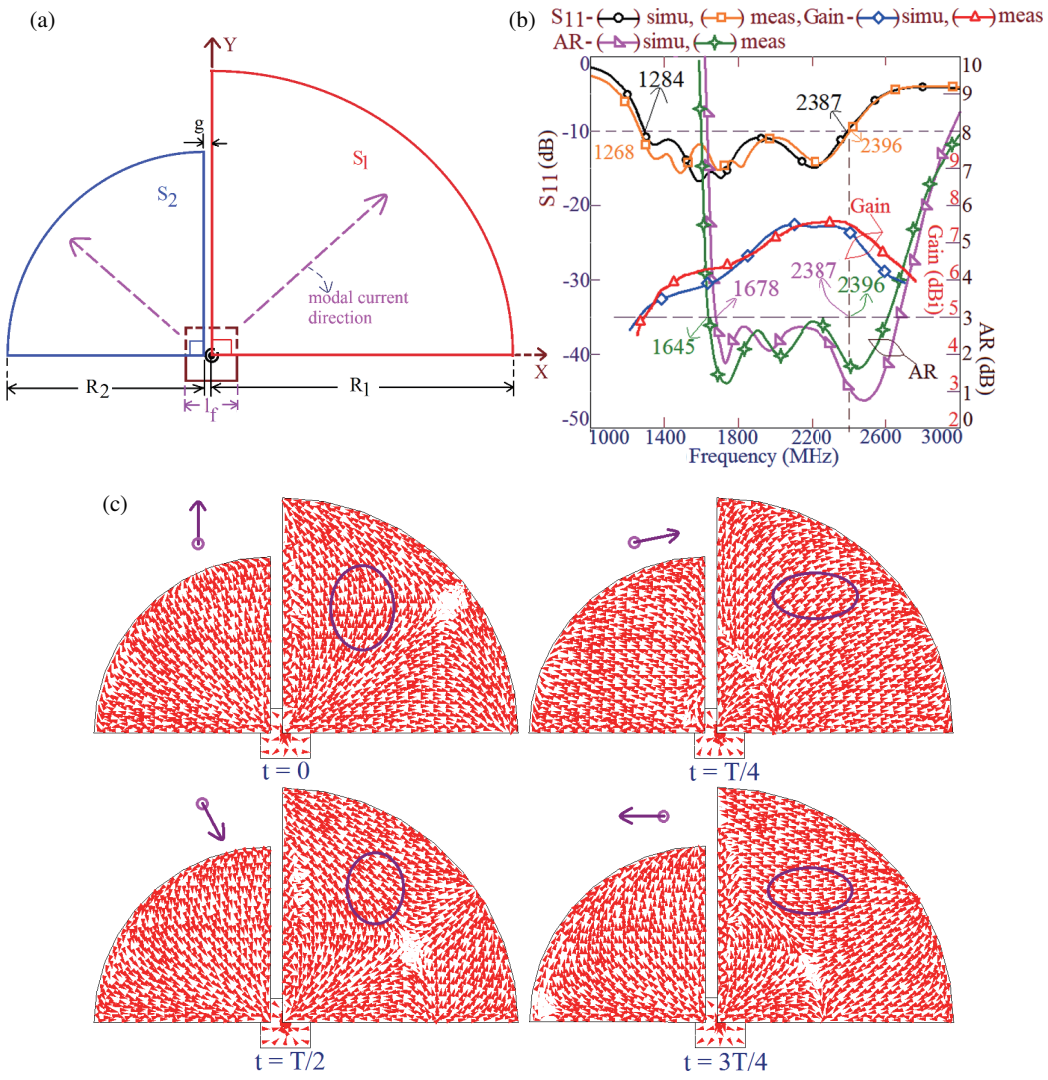

FIGURE 4. (a) Gap-coupled design of 90° S-MSAs, its (b) S_{11} BW and gain plots, its (c)–(e) surface current distribution over the AR BW and its (f) time varying surface current distribution at the center frequency of AR BW.

45° S-MSA, diodes D4 – D6 are forward biased by applying the '+' polarity signal at (3) and '−' polarity signal at (2). As other diodes are not forward biased, they remain off, and thus remaining 45° Sectoral patches are not connected to the fed composite 90° S-MSA. The fabricated prototype of the reconfigurable antenna is shown in Fig. 7(b). This reconfigurable gap-coupled antenna yields simulated BW of 1190 MHz (59.7%), whereas the measured value is 1210 MHz (60%). This BW is lower than that obtained in the design wherein reconfigurable approach is not selected. In the reconfigurable antenna, impedance variation over the patch and that of the resonant cavity increases due to the connection present between the 45° Sectoral patches at a few discrete points. With this, quality factor of the antenna cavity increases that reduces the antenna BW. Since the patches are connected at discrete points through RF diodes, start frequency of the BW is higher.

The gap-coupled configuration of two 90° S-MSAs is realized by connecting '+' polarity of DC bias at (2) & (3) and '−' polarity at (1) and (4). This condition forward biases the diodes D1–D3 and D7–D9. The antenna offers simulated and measured S_{11} BWs of 1096 MHz (52.92%) and 1120 MHz (53%), respectively. Respective simulated and measured AR BWs are 750 MHz (33.33%) and 722 MHz (32.5%). As the connection between the 45° Sectoral patches occurs through the RF diodes, S_{11} BW is lower in this design as well. A marginal change in the AR BW value as compared with the non-reconfigurable design is observed, as AR BW is more dependent on the orthogonality of the resonant mode fields/currents than being dependent on the impedance variation on the Sectoral patches. However, the AR BW is noted in the higher frequency range as against that of non-reconfigurable CP design. The fabricated reconfigurable antenna prototype for CP design is provided in Fig. 7(c). All these reconfigurable designs exhibit similar radiation patterns and gain characteristics to that observed in non-reconfigurable designs. With the exception of S_{11} and AR BW being formed in the higher frequency region, the nature of all the plots for reconfigurable designs is similar to that noted in non-reconfigurable case. Hence, the plots for reconfigurable

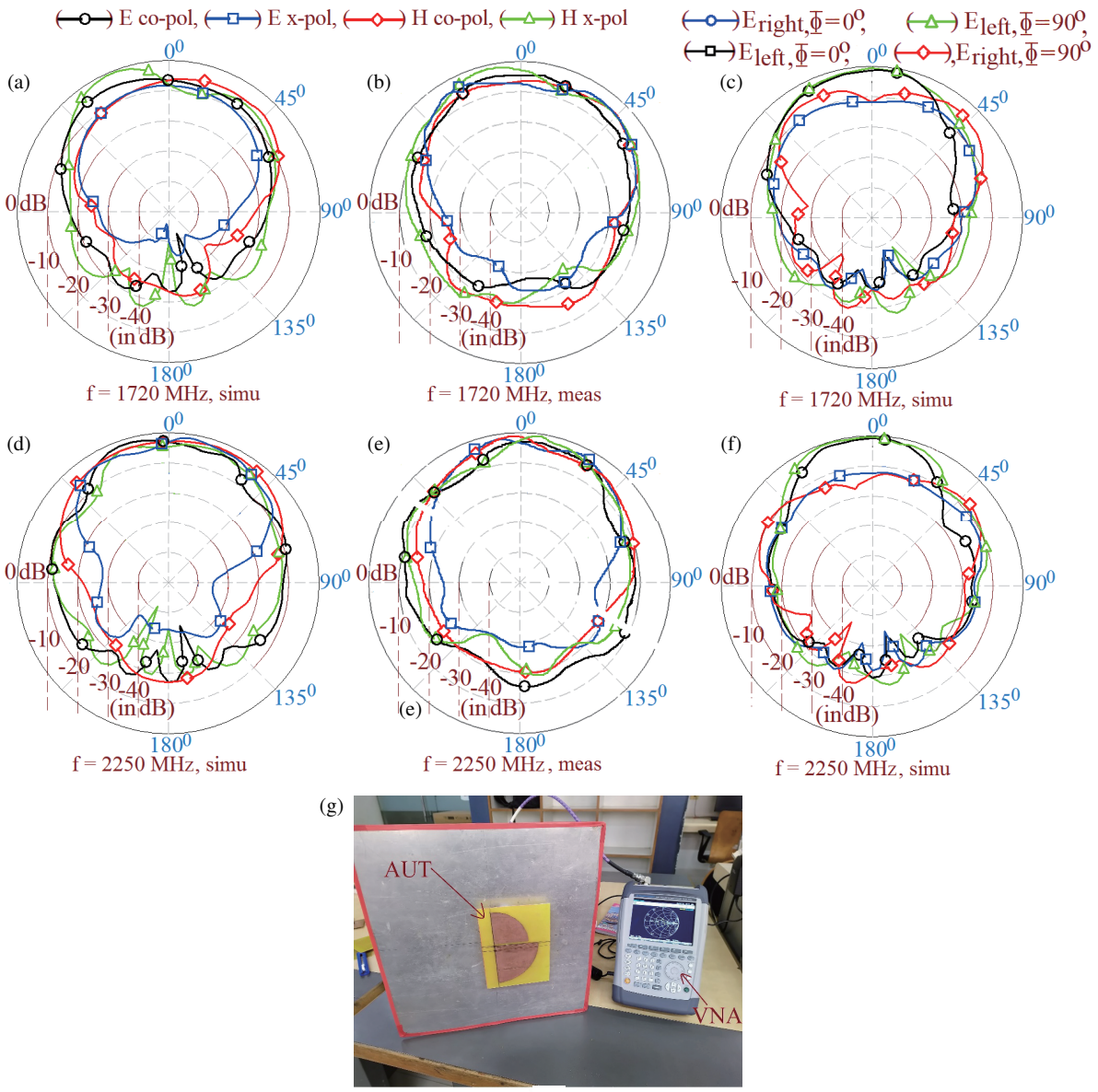

FIGURE 5. Radiation pattern and polarization plots nearer to (a)–(c) band start and (d)–(f) band stop frequency of the AR BW for gap-coupled design of 90° S-MSAs and its (g) impedance measurement setup with the fabricated antenna.

FIGURE 6. Radiation pattern measurement setup with the fabricated antenna.

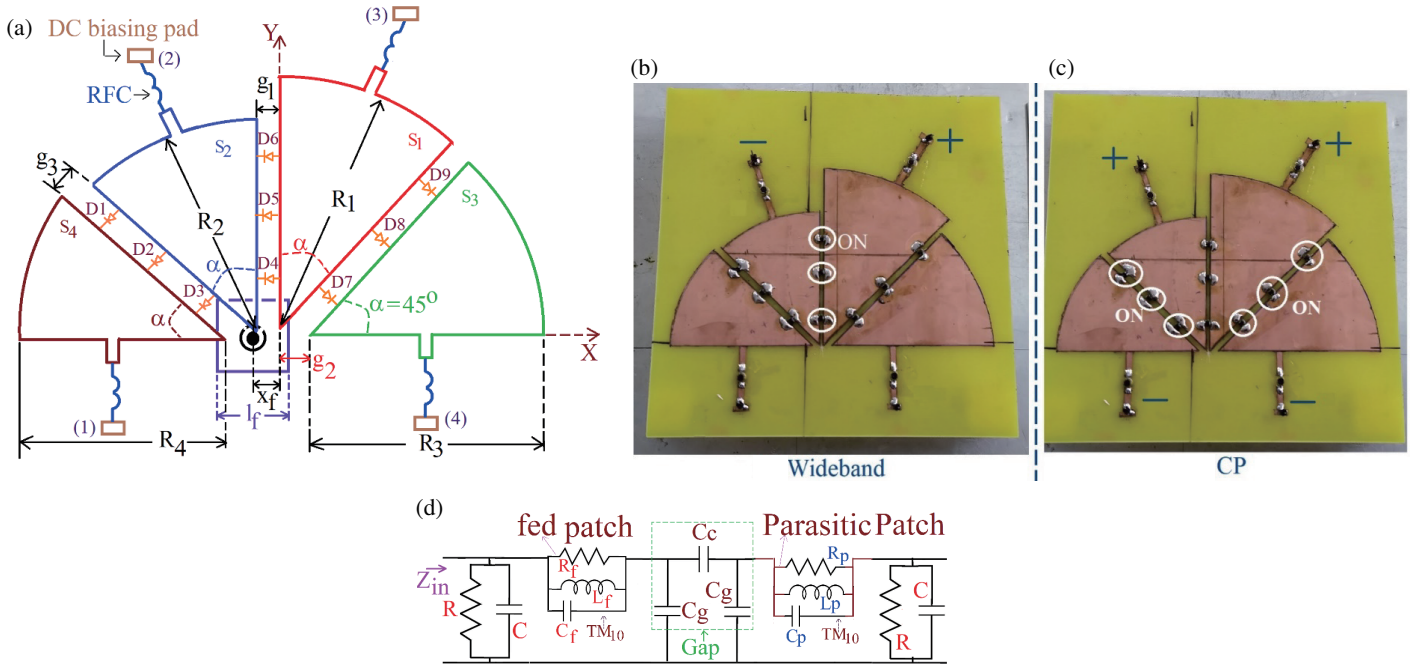

FIGURE 7. (a) Gap-coupled design of reconfigurable 45° S-MSAs, fabricated prototype showing the RF diode excitation for (b) wideband 90° S-MSA with 45° S-MSAs, (c) wideband CP design of 90° S-MSAs, (d) equivalent circuit representation of gap-coupled S-MSAs.

antennas are not provided again. Thus reconfigurable design approach helps to realize wideband and CP response using a single patch, thus avoiding the requirements of multiple antennas. For biasing the RF diode, RFC (ELT3KN131B) is connected to the main patch through connecting lines. It offers either zero impedance for the DC signal in the case of biasing applied or very large impedance at the RF signal. With this, placement of these reconfigurable devices does not affect the functioning of the gap-coupled antenna.

In this study, the analysis of MSA is carried out using resonant mode based approach. In this approach, insights learnt about the resonant modes and their current distributions lead to the correct orientation in between the gap-coupled patches to realize wideband or CP response. Another approach of analyzing the MSAs is an equivalent circuit, and the same for gap-coupled S-MSAs is presented in Fig. 7(d). In this, each of the patches is represented by its parallel resonant circuit at the fundamental TM_{10} mode. The radiation from the gap-coupled antenna is represented by using parallel combination of R, C that represents stored and radiated energies around the gap-coupled patch boundaries. The gap-coupling between the patches is represented by using π-network of capacitors.

5. DESIGN METHODOLOGY FOR CP DESIGN OF GAP-COUPLED 90° S-MSAS

The CP response in gap-coupled 90° S-MSA is because of the optimum frequency spacing between the TM_{10} resonant modes. The resonance curve plots and surface current distributions at the resonant modes in this gap-coupled 90° S-MSAs were studied extensively, and based on the same resonant length formulation at the TM_{10} resonant modes is derived here. For the antenna dimensions in the above gap-coupled design, resonant length at TM_{10} mode in the fed patch is obtained by using Equations (1), (2). R_e represents the effective patch radius, and ε_{re} is the effective dielectric constant for suspended FR4 substrate, which is calculated by using Equation (3). The frequency calculated for the above antenna dimensions using following equation is 1340 MHz that matches closely with the simulated frequency of 1354 MHz. Similarly, resonant length effective patch radius for the gap-coupled patch is obtained by using Equation (4). The second term on the right hand side of Equation (4) that accounts for fringing field extension differs with reference to the resonant length equation for the fed patch. The variation in multiplying factor is attributed to the larger perimeter area in fed patch having higher patch radius. For the above gap-coupled antenna dimensions, frequency calculated using Equations (4) and (1) for $r_e = r_{ep}$ is 1816 MHz that matches closely with the simulated frequency of 1808 MHz. Using these resonant length formulations, the design procedure to achieve the wideband CP response for the given band start frequency of the AR BW is explained further.

$$f_{10fed} = 30/2r_e\sqrt{\varepsilon_{re}} \quad (1)$$

$$r_e = r + 2\,(0.7h_t) \quad (2)$$

$$\varepsilon_{re} = \varepsilon_r\,(h + h_a)\,/h + (h_a\varepsilon_r) \quad (3)$$

$$r_{ep} = r + 2\,(0.5h_t) \quad (4)$$

The procedure is initiated by specifying the band start frequency of the AR BW as f_{AR}. Various frequency relations that exist in between the Sectoral patch resonant mode frequencies and band start frequency of the AR BW, in the above gap-coupled CP design are used in the redesign procedure. Based on these frequency relations, TM_{10} mode frequency of the fed

TABLE 1. Comparison of proposed wideband MSA against reported Wideband designs.

MSA shown in	Measured S_{11} BW (MHz, %)	h/λ_c	A/λ_c (cm)	Peak Gain (dBi)
Fig. 1(a)	**1366, 70.77**	**0.136**	**5.177**	**8.0**
Ref. [3]	350, 6.8	0.04	0.741	7.0
Ref. [4]	290, 8.3	0.035	1.323	6.83
Ref. [5]	490, 20.04	0.053	10.77	9.5
Ref. [6]	374, 5.75	0.068	4.84	—
Ref. [7]	6300, 40	0.119	2.344	10.5
Ref. [8]	905, 42.2	0.233	5.37	10.8
Ref. [9]	380, 14.8	0.049	6.217	9.9
Ref. [10]	260, 13	0.037	5.99	7.0
Ref. [11]	3100, 12	0.1439	0.1649	6.8
Ref. [12]	880, 39.82	0.08	3.1	7.0
Ref. [13]	80, 9	0.04	5.4	7.0
Ref. [14]	7700, 110	0.06	1.83	4.5
Ref. [15]	6900, 86.79	0.065	1.223	4.1

patch is calculated by using Equation (5), whereas Equation (6) relates the TM_{10} mode frequency on gap-coupled patch to AR BW start frequency. For the calculated TM_{10} mode frequency on fed patch, a substrate of thickness h_t is selected as per Equation (7). An air suspended FR4 substrate is used in the redesign, and hence the initial value of the effective dielectric constant (ε_{re}) is unknown. Based on the substrate parameters and thickness present in the original design above, the initial approximation of $\varepsilon_{re} = 1.05$ is considered. Using this total substrate thickness h_t is calculated. This equals $h + h_a$, where h_a is the air gap thickness. For this calculated value h_t and for FR4 substrate ($h = 0.16$ cm), practically realizable and integer value of air gap thickness h_a is chosen. Using the values of h and h_a, ε_{re} is recalculated using Equation (3), which is used in all further calculations. Further, fed and parasitic patch radii are calculated by using Equations (8) and (9), respectively. A square proximity strip of dimension $l_f = 0.0786\lambda_g$ is placed at a thickness of $h_s = 0.0694\lambda_g$ above the ground plane. The strip is placed exactly below the vertex point of fed Sectoral patch as shown in Fig. 4(a). The air gap between the two Sectoral patches is kept equal to $g = 0.1942h_t$.

$$f_{10fed} = f_{AR}/1.255 \quad (5)$$

$$f_{10p} = f_{AR}/0.9402 \quad (6)$$

$$h_t = 0.095\,(30/f_{10fed}\sqrt{\varepsilon_{re}}) \quad (7)$$

$$r = \left(30/2f_{10fed}\sqrt{\varepsilon_{re}}\right) - 1.4\,(h + h_a) \quad (8)$$

$$r_p = \left(30/2f_{10fed}\sqrt{\varepsilon_{re}}\right) - 1.0\,(h + h_a) \quad (9)$$

With reference to Fig. 4(a), $r = R_1$ and $r_p = R_2$, here. Using these equations and design procedure, the gap-coupled configuration of two 90° S-MSAs is designed for $f_{AR} = 1100$ MHz, so as to cover GPS L-band frequencies. Various antenna parameters calculated are $h_a = 3.0$, $h = 0.16$, $r = 12.35$, $r_p = 9.4$, $h_s = 2.3$, $l_f = 2.65$ cm. The antenna offers simulated and measured S_{11} BWs of 668 MHz (56.23%) and 681 MHz (56.9%), respectively. Simulated and measured values of the CP BW for AR $\leq$ 3 dB, which completely lies inside the $S_{11} \leq -10$ dB, are 414 MHz (31.48%) and 424 MHz (31.98%), respectively. The AR BW in two results completely spans GPS L2 and L5 bands. The CP antenna offers the gain above 6 dBi over the AR BW with a peak value of 7 dBi. The nature of plots in the redesigned antenna for S_{11} & AR BW, radiation pattern, and gain is similar to those observed in above original gap-coupled S-MSAs. Thus, to avoid the repeatability in results, they are not shown for redesigned S-MSA. Using the proposed design methodology, a wideband gap-coupled CP MSA can be realized as per specific wireless application.

6. RESULTS DISCUSSION AND COMPARATIVE ANALYSIS

Among the proposed Sectoral MSAs, the wideband design of 90° S-MSA with 45° S-MSAs offers the BW of nearly 70% whereas gap-coupled CP design yields AR BW of 34%. To put forward the technical novelty in the proposed work, the comparison of these two designs against the reported wideband and CP configurations is presented in this section. The comparison, as given in Tables 1 & 2, is presented for the measured S_{11} or AR BW, peak gain, and antenna volume, i.e., substrate thickness and patch area. In the wideband configurations, patch area and substrate thickness are normalized with reference to the center frequency of S_{11} BW, whereas in CP designs, they are normalized with reference to the center frequency of AR BW. This normalization helps in comparing different configurations, which are being optimized in different frequency spectra and substrate parameters.

The wideband designs discussed in [3, 4] are optimized on thinner substrate and offer lower impedance BW than gap-coupled 90° S-MSA with 45° S-MSAs configuration. The wideband design presented in [5] required larger patch area be-

TABLE 2. Comparison of proposed wideband CP S-MSA against reported CP designs.

MSA shown in	Measured AR BW (MHz, %)	h/λ_{AR}	A/λ_{AR} (cm)	Peak Gain (dBi)
Fig. 3(a)	**751, 37.12**	**0.129**	**4.915**	**7.5**
Ref. [16]	23, 0.93	0.02	1.498	3.87
Ref. [17]	18, 0.72	0.04	2.23	6.03
Ref. [18]	16, 0.653	0.04	3.5	7.6
Ref. [19]	46, 3.9	0.01	4.97	3.45°
Ref. [20]	8, 0.5	0.02	5.64	3.9
Ref. [22]	6, 0.4	0.05	1.36	2.3
Ref. [24]	1000, 19	0.12	3.54	7.5
Ref. [25]	1160, 21.05	0.183	0.506	8.0
Ref. [26]	160, 8.2	0.067	1.352	7.0
Ref. [28]	3040, 63.7	0.101	38.3	17.77
Ref. [29]	250, 7.13	0.052	3.856	7.75

cause of the parasitic elements being used. The gap-coupled design presented in [6] has lower gain as it is fabricated on a lossy thinner substrate. The gap-coupled configuration of rectangular patch with shorted patch elements [7] offers lower BW than the proposed wideband design. The wideband multi-resonator design discussed in [8] offers higher gain but requires patches in planar and stacked layer. This increases the overall antenna volume. The dual slot cut Rectangular MSA (RMSA) discussed in [9] offers lower S_{11} BW, whereas the wideband design presented in [10] employs differential feeding. Compared to the configuration discussed in [10], the proposed configuration employs simpler proximity feeding. In spite of two U-slots being employed in [11], the reported design offers a BW less than 15%. Three rectangular slots are employed in the wideband design discussed in [12]. With three slots, multiple resonant modes are expected to be present in this configuration. However, the multiple slots cut design offers lower BW than the proposed configuration. A novel technique is reported to reduce the antenna thickness in wideband E-shape design presented in [13]. However, the printed patch element which is employed to reduce the substrate thickness is complex in design, and the configuration has lower S_{11} BW. The defected ground plane designs discussed in [14, 15] employ either multiple patches on the patch and ground plane or only the slot cut ground plane. Due to this modified ground plane, these designs have lower antenna gain. The S_{11} BW as offered by the slots cut ground plane design that is backing rectangular patch [42] is lower than that obtained in the proposed wideband design.

The CP designs discussed in [16–20], which employ either narrow slot, stub, shorting post, or modified patch shapes, offer much lower AR BW than the proposed design. The gain reported in shorted design discussed in [18] is larger, but in this work, that of the shorted patch modes yielding CP response is not discussed. The modified patch shape CP design employing proximity feeding discussed in [21] requires a thicker substrate and offers only 5–6% of AR BW. The U-slot ground plane design with fractal iterations discussed in [22, 23] has narrow AR BW ($\leq$ 2%). Multiple slots cut modified shape CP design discussed in [24] offers lower AR BW than the simpler gap-coupled CP design proposed in this work. The triple mode configuration employing unequal length U-slot for CP response is discussed in [25]. It provides lower AR BW than the proposed gap-coupled design. In addition, that of the third additional mode adding to AR BW against the earlier reported unequal length U-slot cut CP MSA and design methodology to realize triple mode CP configuration around specific frequency band is not discussed. The multi-layer stacked ring design discussed in [26] and gap-coupled design presented in [27] have lower AR BW than the proposed gap-coupled design of Sectoral patches. The CP design presented in [28] offers higher AR BW and gain, but it requires large patch size due to the array configuration. In spite of employing four resonators in the gap-coupled configuration discussed in [29], the reported AR BW is smaller.

In the literature using active elements various reconfigurable designs have been reported which achieve either wideband response with a pattern reconfigurable radiation characteristics [30, 32], or orthogonal polarization across the operating bands [31], or broadside to end-fire direction and linear to CP response switchable pattern characteristics using a high gain antenna array [33, 34]. However, these MSAs employ differential feeding that makes the design complex in implementation, or thinner substrate which yields lower BW, or higher patch size attributed to the modified ground plane or array design. The requirement of power divider circuit adds to the design complexities in an array configuration. Against these and various reported reconfigurable designs, the proposed MSAs as well as their reconfigurable variation offer higher impedance and AR BW with an appreciably higher value of antenna gain. They use simpler gap coupled technique in combination with a proximity feed, thus making it a design friendly configuration. Using modified variations of Sectoral patches, wideband and CP variations are reported [35–40]. However, in these designs, lower impedance or AR BW is observed. These configurations do not involve the reconfigurable approach to realize switching in between wideband and CP characteristics in the single patch configuration.

In the present study, by using a simple gap-coupled technique in combination with the proximity feed, wideband linearly polarized and circularly polarized configurations involving 90° and 45° S-MSAs are proposed. The respective designs yield BWs of greater than 65% and 30% with a gain above 6 dBi. The reconfigurable design is presented that helps in realizing wideband and CP characteristics using a single patch configuration. Design methodology for CP antenna is put forward that helps in realizing wideband CP MSA as per specific frequency band, which can be as per given wireless application. Thus, a simpler wideband configuration of 90° and 45° S-MSAs, offering reconfigurable characteristics for wideband and CP response, is the new contribution in the proposed work.

7. CONCLUSIONS

Gap-coupled variations of 90° and 45° S-MSAs for wideband and circularly polarized response are proposed. The wideband design involving 90° and 45° S-MSAs offers an impedance BW of $\sim$ 70%, whereas the CP design with two 90° S-MSAs offers an AR BW of 34%. Both optimum designs offer broadside pattern characteristics with a gain above 6 dBi across the S_{11} and AR BW. To achieve both responses using a single patch, a reconfigurable design involving active elements that offer similar antenna characteristics is proposed. A design methodology is presented to achieve a wideband CP response around a specific frequency band. This approach helps in designing wideband CP S-MSA as per specific wireless applications. Thus, simpler designs of 90° and 45° S-MSAs that offer either wideband linearly polarized or CP response with an option of the reconfigurable design approach are the new technical contributions in the present work.

ACKNOWLEDGEMENT

The proposed reconfigurable gapcoupled design is published with application number 202321080257A, under the title "Reconfigurable Sectoral Microstrip Antennas For Wideband And Circularly Polarized Response", in The Indian Patent Office Journal No. 02/2024 Dated 12/01/2024.

REFERENCES

[1] Garg, R., *Microstrip Antenna Design Handbook*, Artech House, 2001.

[2] Kumar, G. and K. P. Ray, *Broadband Microstrip Antennas*, Artech House, 2002.

[3] Yoo, J.-U. and H.-W. Son, "A simple compact wideband microstrip antenna consisting of three staggered patches," *IEEE Antennas and Wireless Propagation Letters*, Vol. 19, No. 12, 2038–2042, 2020.

[4] Qian, J.-F., F.-C. Chen, Q.-X. Chu, Q. Xue, and M. J. Lancaster, "A novel electric and magnetic gap-coupled broadband patch antenna with improved selectivity and its application in MIMO system," *IEEE Transactions on Antennas and Propagation*, Vol. 66, No. 10, 5625–5629, 2018.

[5] Yang, D., H. Zhai, C. Guo, and H. Li, "A compact single-layer wideband microstrip antenna with filtering performance," *IEEE Antennas and Wireless Propagation Letters*, Vol. 19, No. 5, 801–805, 2020.

[6] Balaji, U., "Bandwidth enhanced circular and annular ring sectoral patch antennas," *Progress In Electromagnetics Research Letters*, Vol. 84, 67–73, 2019.

[7] Cao, Y., Y. Cai, W. Cao, B. Xi, Z. Qian, T. Wu, and L. Zhu, "Broadband and high-gain microstrip patch antenna loaded with parasitic mushroom-type structure," *IEEE Antennas and Wireless Propagation Letters*, Vol. 18, No. 7, 1405–1409, 2019.

[8] Chopra, R. and G. Kumar, "High gain broadband stacked triangular microstrip antennas," *Microwave and Optical Technology Letters*, Vol. 62, No. 9, 2881–2888, 2020.

[9] Liu, N.-W., L. Zhu, W.-W. Choi, and G. Fu, "A low-profile wideband aperture-fed microstrip antenna with improved radiation patterns," *IEEE Transactions on Antennas and Propagation*, Vol. 67, No. 1, 562–567, 2019.

[10] Liu, N.-W., L. Zhu, and W.-W. Choi, "A differential-fed microstrip patch antenna with bandwidth enhancement under operation of TM_{10} and TM_{30} modes," *IEEE Transactions on Antennas and Propagation*, Vol. 65, No. 4, 1607–1614, 2017.

[11] Fan, T.-Q., B. Jiang, R. Liu, J. Xiu, Y. Lin, and H. Xu, "A novel double U-slot microstrip patch antenna design for low-profile and broad bandwidth applications," *IEEE Transactions on Antennas and Propagation*, Vol. 70, No. 4, 2543–2549, 2022.

[12] Li, W.-W., Q.-H. Li, Y. Meng, J.-Y. Wang, and W.-M. Xu, "A broadband microstrip patch antenna with multiple open slots," *Microwave and Optical Technology Letters*, Vol. 61, No. 3, 626–632, 2019.

[13] Chen, Y., S. Yang, and Z. Nie, "Bandwidth enhancement method for low profile E-shaped microstrip patch antennas," *IEEE Transactions on Antennas and Propagation*, Vol. 58, No. 7, 2442–2447, 2010.

[14] Baudha, S. and M. V. Yadav, "A novel design of a planar antenna with modified patch and defective ground plane for ultra-wideband applications," *Microwave and Optical Technology Letters*, Vol. 61, No. 5, 1320–1327, 2019.

[15] Mandal, K. and P. P. Sarkar, "High gain wide-band U-shaped patch antennas with modified ground planes," *IEEE Transactions on Antennas and Propagation*, Vol. 61, No. 4, 2279–2282, 2013.

[16] Ray, M. K., K. Mandal, and N. Nasimuddin, "Low-profile circularly polarized patch antenna with wide 3 dB beamwidth," *IEEE Antennas and Wireless Propagation Letters*, Vol. 18, No. 12, 2473–2477, 2019.

[17] Zhao, Z., F. Liu, J. Ren, Y. Liu, and Y. Yin, "Dual-sense circularly polarized antenna with a dual-coupled line," *IEEE Antennas and Wireless Propagation Letters*, Vol. 19, No. 8, 1415–1419, 2020.

[18] Zhang, X., L. Zhu, and N.-W. Liu, "Pin-loaded circularly-polarized patch antennas with wide 3-dB axial ratio beamwidth," *IEEE Transactions on Antennas and Propagation*, Vol. 65, No. 2, 521–528, 2017.

[19] Agrawal, N., A. K. Gautam, and R. Mishra, "Design of low volume circularly polarized annular ring-shaped planar antenna for GPS applications," *International Journal of RF and Microwave Computer-Aided Engineering*, Vol. 31, No. 7, e22698, 2021.

[20] Shi, Y. and J. Liu, "A circularly polarized octagon-star-shaped microstrip patch antenna with conical radiation pattern," *IEEE Transactions on Antennas and Propagation*, Vol. 66, No. 4, 2073–2078, 2018.

[21] Deshmukh, A. A. and K. P. Ray, "Circularly polarized designs of modified isosceles triangular microstrip antennas," *Engineering Reports*, Vol. 2, No. 10, e12250, 2020.

[22] Wei, K., J. Y. Li, L. Wang, R. Xu, and Z. J. Xing, "A new technique to design circularly polarized microstrip antenna by fractal defected ground structure," *IEEE Transactions on Antennas and*

Propagation, Vol. 65, No. 7, 3721–3725, 2017.

[23] Ambekar, A. G. and A. A. Deshmukh, "Low profile design of regular shape microstrip antennas backed by fractal slots cut ground plane for circular polarized response," *Progress In Electromagnetics Research C*, Vol. 129, 203–219, 2023.

[24] Mondal, T., S. Maity, R. Ghatak, and S. R. B. Chaudhuri, "Design and analysis of a wideband circularly polarised perturbed psi-shaped antenna," *IET Microwaves, Antennas & Propagation*, Vol. 12, No. 9, 1582–1586, 2018.

[25] Zeng, J., X. Liang, L. He, F. Guan, F. H. Lin, and J. Zi, "Single-fed triple-mode wideband circularly polarized microstrip antennas using characteristic mode analysis," *IEEE Transactions on Antennas and Propagation*, Vol. 70, No. 2, 846–855, 2022.

[26] Cheng, G., B. Huang, Z. Huang, and L. Yang, "A high-gain circularly polarized filtering stacked patch antenna," *IEEE Antennas and Wireless Propagation Letters*, Vol. 22, No. 5, 995–999, 2023.

[27] Dash, S. K. K., Q. S. Cheng, and T. Khan, "An off-center-fed compact wideband antenna with truncated corners and parasitic patches for circular polarization," *International Journal of RF and Microwave Computer-Aided Engineering*, Vol. 30, No. 8, e22244, 2020.

[28] Verma, A., M. Arrawatia, and G. Kumar, "High gain wideband circularly polarized microstrip antenna array," *IEEE Transactions on Antennas and Propagation*, Vol. 70, No. 11, 11 183–11 187, 2022.

[29] Wu, Q.-S., X.-Y. Tang, X. Zhang, L. Zhu, G. Zhang, and C.-B. Guo, "Circularly-polarized patch antennas with enhanced bandwidth based on capacitively coupled orthogonal patch radiators," *IEEE Open Journal of Antennas and Propagation*, Vol. 4, 472–483, 2023.

[30] Radavaram, S. and M. Pour, "Wideband radiation reconfigurable microstrip patch antenna loaded with two inverted U-slots," *IEEE Transactions on Antennas and Propagation*, Vol. 67, No. 3, 1501–1508, 2018.

[31] Hong, K.-D., X. Chen, X. Zhang, L. Zhu, and T. Yuan, "A slot-loaded high-gain circular patch antenna with reconfigurable orthogonal polarizations and low cross polarization," *IEEE Antennas and Wireless Propagation Letters*, Vol. 21, No. 3, 511–515, 2022.

[32] Qin, P.-Y., Y. J. Guo, A. R. Weily, and C.-H. Liang, "A pattern reconfigurable U-slot antenna and its applications in MIMO systems," *IEEE Transactions on Antennas and Propagation*, Vol. 60, No. 2, 516–528, 2011.

[33] Omar, A. A., J. Choi, J. Kim, J. Park, B. Seong, J. Lee, and W. Hong, "A planar, polarization-switchable endfire and±broadside millimeter-wave antenna array without lumped components," *IEEE Transactions on Antennas and Propagation*, Vol. 70, No. 5, 3864–3869, 2022.

[34] Kim, K.-B., B. C. Jung, and J.-M. Woo, "A compact dual-polarized (CP, LP) with dual-feed microstrip patch array for target detection," *IEEE Antennas and Wireless Propagation Letters*, Vol. 19, No. 4, 517–521, 2020.

[35] Deshmukh, A. A. and N. V. Phatak, "Broadband sectoral microstrip antennas," *IEEE Antennas and Wireless Propagation Letters*, Vol. 14, 727–730, 2014.

[36] Deshmukh, A. A. and N. V. Phatak, "Analysis and design of broadband 90° sectoral microstrip antennas," *Microwave and Optical Technology Letters*, Vol. 58, No. 4, 927–932, 2016.

[37] Deshmukh, A. A., T. Sawant, and A. G. Ambekar, "Wideband and circularly polarized variations of sectoral microstrip antennas," in *Proceedings of International Conference on Wireless Communication: ICWiCOM 2021*, 29–37, 2022.

[38] Lu, W.-J., Q. Li, S.-G. Wang, and L. Zhu, "Design approach to a novel dual-mode wideband circular sector patch antenna," *IEEE Transactions on Antennas and Propagation*, Vol. 65, No. 10, 4980–4990, 2017.

[39] Yu, J., W.-J. Lu, Y. Cheng, and L. Zhu, "Tilted circularly polarized beam microstrip antenna with miniaturized circular sector patch under wideband dual-mode resonance," *IEEE Transactions on Antennas and Propagation*, Vol. 68, No. 9, 6580–6590, 2020.

[40] Wu, Z.-F., W.-J. Lu, J. Yu, and L. Zhu, "Wideband null frequency scanning circular sector patch antenna under triple resonance," *IEEE Transactions on Antennas and Propagation*, Vol. 68, No. 11, 7266–7274, 2020.

[41] IE3D 12.1, Zealand software, 2007.

[42] Sener, G., "A novel compact rectangular microstrip patch antenna with a superstrate element for 2.4 GHz WLAN applications," *Academic Perspective Procedia*, Vol. 3, No. 1, 538–542, 2020.